Heritage Science

RESEARCH

Open Access

Recognition of Yuan blue and white porcelain produced in Jingdezhen based on graph anomaly detection combining portable X-ray fluorescence spectrometry

Jinwei Li[1,2], Yifei Yang[3,4*], Dongmian Zou[4*], Lin Wu[1], Qiang Wu[1], Ziwei Lin[1] and Qijiang Li[1,2]

Abstract

The blue and white porcelain produced in Jingdezhen during China's Yuan Dynasty is an outstanding cultural heritage of ceramic art that has attracted wide attention for its identification. However, the traditional visual identification method is susceptible to misjudgment, thermoluminescence dating damages the samples, and the methods based on chemical analysis are limited by the accuracy and specificity of the elemental features. In this paper, we address the identification challenge by using machine learning techniques combined with portable X-ray Fluorescence Spectrometer (pXRF) analysis. We collect a large dataset of chemical compositions of Yuan blue and white porcelain from Jingdezhen using pXRF, and propose a graph anomaly detection method based on gradient attention map (GRAM) to identify the porcelain from different dynasties. We treat the porcelain produced in the Yuan dynasty as normal samples and those from other dynasties as abnormal samples. For GRAM, we merely train the variational graph autoencoder (VGAE) model with normal graphs and then use its encoder to extract graph features and compute the anomaly scores by utilizing the GRAM of the graph representations with respect to the node feature embeddings. Finally, we compare GRAM with state-of-the-art graph anomaly detection techniques and show that it achieves superior performance.

Keywords Blue and white porcelain, Ancient ceramic identification, Portable X-ray Fluorescence Spectrometer analysis, Anomaly detection, Graph neural networks

Introduction

Blue and white porcelain is the most renowned variety of ceramics in China, famous worldwide for its skillful combination of blue underglaze color and white porcelain body. It belongs to the category of underglaze colored porcelain, which is produced by painting patterns on the ceramic body with cobalt-containing pigments, covering it with a layer of transparent glaze, and firing it at high temperatures in a reducing kiln [1]. The successful firing of blue and white porcelain in Jingdezhen during the Yuan Dynasty (1271–1368 A.D.) of China marked a new phase in the development of the Chinese ceramic industry, dominated by polychrome porcelain, which provided a rich cultural heritage for the innovation

*Correspondence:
Yifei Yang
yfyang@whu.edu.cn
Dongmian Zou
dongmian.zou@duke.edu
[1] Research Center of Ancient Ceramic, Jingdezhen Ceramic University, Jingdezhen 333001, China
[2] Jiangxi Ceramic Heritage Conservation and Imperial Kiln Research Collaborative Innovation Center, Jingdezhen 333001, China
[3] Electronic Information School, Wuhan University, Wuhan 430072, China
[4] Zu Chongzhi Center for Mathematics and Computational Sciences and Data Science Research Center, Duke Kunshan University, Kunshan 215316, China

and development of ceramic art [2]. Moreover, it facilitated international trade and cultural exchanges between China and the rest of the world, thereby consolidating Jingdezhen as a national ceramic center and playing a vital role in making China a world-famous ceramic nation [2, 3].

The identification of Yuan blue and white porcelain, which has attracted increasing attention, is a crucial area of research. Traditional visual identification relies mainly on typological features such as vessel shape, glaze color, and decorative patterns. However, this approach has limitations, as human senses cannot access the microstructural aspects of ceramics. Furthermore, the different levels of expertise of appraisers can lead to uncertainties in understanding and evaluating ceramics, which may cause misjudgments or errors. Currently, thermoluminescence dating can provide the absolute age of porcelain for identification [4], but this method requires damaging the ceramic bodies. Chemical composition analysis is another method for determining the provenance and dating of ancient ceramics, based on the underlying principle that ceramics from different periods and kilns in ancient China exhibit distinct chemical compositions due to variations in formulas. Currently, various analytical techniques are utilized for testing ceramic chemical composition, including Atomic absorption spectroscopy (AAS), Neutron activation analysis (NAA), Proton Induced X-ray emission (PIXE), Inductively coupled plasma-mass spectrometry (ICP-MS), X-ray fluorescence spectrometry (XRF), Laser-induced breakdown spectroscopy (LIBS), etc. Among these, portable X-ray Fluorescence Spectrometer (pXRF) is a handheld and non-destructive device that enables the measurement of elemental composition of archaeological artifacts, making it particularly suitable for use in archaeological sites and museum collections [5, 6]. The pXRF analysis can provide valuable information for the preservation and authentication of ceramics, as it can reveal the differences in the chemical compositions of ceramics from different historical periods, which reflect the varying formulas used for producing ceramics in the same region [7–11]. However, this method of chemical composition comparison also has some drawbacks, such as the emphasis on specific elemental features (e.g., Ca, Al, Si, Fe, Co) and the overlap in the chemical compositions of ceramics from different periods [8, 11]. Therefore, there is a need for further improvements in accuracy.

Machine learning, driven by data availability and computational scale, offers new opportunities for developments and applications in ancient ceramic identification. For example, neural networks were used to recognize handwritten Chinese characters in images of ancient ceramics [12], and to classify ancient celadons of different kilns [13] and black glazed wares of Jian kilns [14] utilizing datasets of chemical compositions measured from ceramic bodies and glazes.

This work uses pXRF to obtain a large amount of chemical composition data of Yuan blue and white porcelain produced in Jingdezhen. The aim is to address the challenges of ancient ceramic identification using machine learning techniques combined with pXRF analysis. The problem is formulated as an anomaly detection task, where the model determines whether a porcelain sample was produced during the Yuan Dynasty or not. Porcelain samples from the Yuan Dynasty are considered as normal samples, and porcelain samples from other dynasties are considered as abnormal samples. Thus, the original problem is abstracted as an anomaly detection problem.

Anomalies refer to instances or situations that significantly deviate from anticipated behavior. Traditional anomaly detection methods rely on feature representations of data to detect anomalies [15–18]. With the increasing prominence of deep learning, neural networks have emerged as powerful tools to extract complex and meaningful patterns from high-dimensional data, improving anomaly detection performance [19–22]. These methods, however, often disregard the intrinsic relational information embedded within real-world data, focusing only on outliers in the feature space. This leads to suboptimal results, especially in challenging scenarios. In our task, we deal with data that has different but related components, requiring us to consider their relations when applying machine learning techniques. Graph Neural Networks (GNNs) constitute a class of neural models that can capture intricate insights from both graph structures and node attributes, positioning them as promising solutions for tackling Graph Anomaly Detection (GAD) tasks. GNN-based GAD methods have grown rapidly in recent years [23–27]. Nevertheless, these methods lack interpretability and reliability in real scenarios. Therefore, we propose a novel GNN interpretation approach that aligns most effectively with the characteristics of our specific dataset.

Materials and methods

Datasets

All porcelain samples in this study were provided by the Yuan Blue and White Museum of Jingdezhen Ceramic University. This study analyzes the chemical composition data of 233 blue and white porcelains from the Yuan Dynasty, produced in Jingdezhen. Among the 233 Yuan blue and white porcelains, 160 samples are intact objects that have undergone meticulous plaster restoration. These objects encompass plates, bowls, jars, vases, and cups. Additional file 1: Appendix S1 provides a detailed description of some representative objects. The

Fig. 1 Photos of Yuan blue and white porcelain shards produced in Jingdezhen

remaining porcelains are unrepaired shards. It is worth noting that during the selection process for unrepaired shards, we prioritized larger ones and conducted thorough pattern and typology comparisons to ensure they come from different porcelain objects (Fig. 1). For comparison, 24 blue and white porcelain shards from the Chenghua Reign of Ming Dynasty to the Daoguang Reign of Qing Dynasty (1465–1850 A.D.), also made in Jingdezhen, were included.

The chemical compositions of the body, glaze, and blue area of the samples were measured non-destructively by a Bruck TRACER 5 pXRF instrument at the Research Center of Ancient Ceramic, Jingdezhen Ceramic University, Jingdezhen. The measurements were performed under the same experimental conditions: 20 kV voltage, 200 μA current, vacuum environment, and 3 mm spot size. To reduce measurement error, four points of the

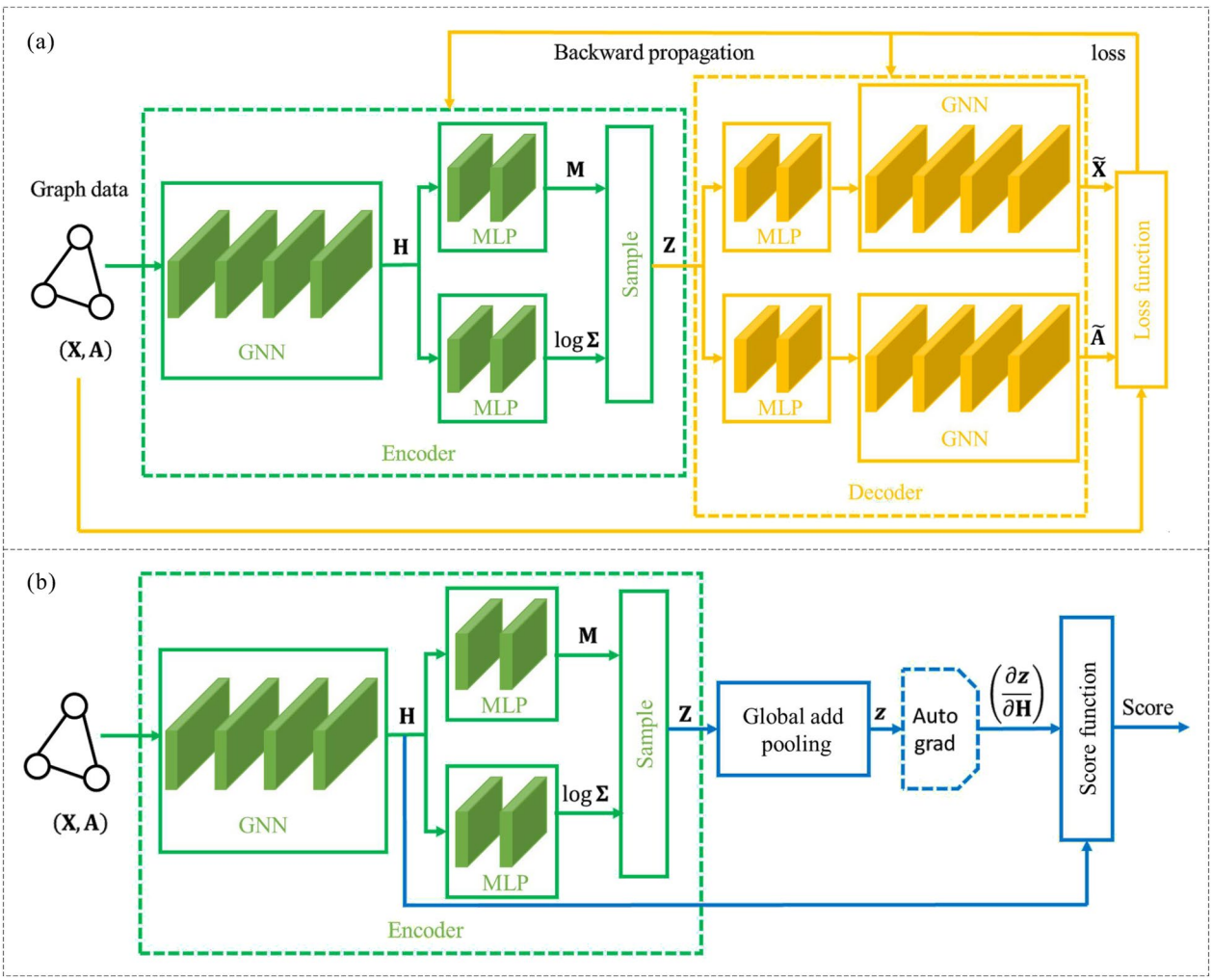

Fig. 2 The framework of the GRAM based on the VGAE model. **a** Training phase: The VGAE model is trained according to the reconstruction error. **b** Testing phase: The encoder is employed to compute the anomaly score

same type in each sample were analyzed and averaged. We performed pXRF on the homogeneous and non-porous surfaces of the body, uncolored glaze, and blue area, and excluded the corroded area from the analysis to ensure the reliability of the results [28]. When determining the chemical compositions of the blue area in blue and white porcelain, we generally choose the areas with deep blue color for testing, while avoid the black iron spots. The spectrum collection time for each spot was 200 s. The whole experiment is consistent with Wu et al. [29]. A set of 13 standard samples for XRF analysis of ancient porcelains, developed by the Shanghai Institute of Ceramics, Chinese Academy of Sciences, was used to establish the calibration curves of each element [29, 30]. The accuracy and precision of the results were monitored by the national standard material GBW07402 (clay). The relative standard deviation (RSD) of the concentrations of the oxides was less than 5%. The relative error was less than 10% for P_2O_5 and less than 5% for other oxides. The detection limit of the measured oxides was approximately 0.1 wt%.

This study uses the chemical composition data of three components: body, glaze, and blue area. The body and glaze components were measured for ten elements (Na_2O, MgO, Al_2O_3, SiO_2, P_2O_5, K_2O, CaO, TiO_2, MnO, and Fe_2O_3). The blue area patterns were irregular and sometimes smaller than the pXRF spot size, resulting in mixed data with the glaze matrix. A dilution ratio correction method [31, 32] was used to estimate the actual CoO contents and ratios of MnO/CoO and Fe_2O_3/CoO of the cobalt blue area. CaO in the blue area indicated the glaze dilution, as the glaze had much higher calcium contents than the cobalt-containing materials [1]. The dilution ratios were calculated using formula (1), and the corrected ratios of MnO, Fe_2O_3, and CoO were calculated using formula (2) and formula (3). The parameters of oxides in formulas (1–3) represent the weight percentage. Hence, the blue area component was measured for an extended set of CoO, MnO/CoO, and Fe_2O_3/CoO.

$$\mathrm{d} = \frac{|\mathrm{PCaO} - \mathrm{GCaO}|}{\mathrm{PCaO}} \tag{1}$$

$$\frac{\mathrm{MnO}}{\mathrm{CoO}} = \left| \frac{\mathrm{PMnO} \times (\mathrm{d}+1) - \mathrm{GMnO}}{\mathrm{PCoO} \times (\mathrm{d}+1)} \right| \tag{2}$$

$$\frac{\mathrm{Fe_2O_3}}{\mathrm{CoO}} = \left| \frac{\mathrm{PFe_2O_3} \times (\mathrm{d}+1) - \mathrm{GFe_2O_3}}{\mathrm{PCoO} \times (\mathrm{d}+1)} \right| \tag{3}$$

d = dilution ratio, P = blue area, G = glaze.

Machine learning methodology

This work aims to discriminate whether an ancient ceramic sample was produced during the Yuan Dynasty or not. We laber ceramic samples from the Yuan Dynasty as normal samples and ceramic samples from other dynasties as abnormal samples.

To solve this anomaly detection problem, we construct a graph-based dataset of blue and white porcelains from the Yuan Dynasty. We treat each component as a node in the graph, and use 11 chemical compositions (Na_2O, MgO, Al_2O_3, SiO_2, P_2O_5, K_2O, CaO, TiO_2, MnO, Fe_2O_3, and CoO) and 2 revised ratios (MnO/CoO and Fe_2O_3/CoO) as node features $\mathbf{X}$, resulting in a total of 13 dimensions. We pad the missing CoO and the revised ratios (MnO/CoO and Fe_2O_3/CoO) for the body and glaze components with zeros. To account for structural information $\mathbf{A}$, we connected each node using undirected edges, thereby constructing a fully connected undirected graph. Overall, our dataset consists of 257 sets of data, comprising 233 normal cases from Yuan Dynasty samples and 24 anomalous cases from other dynasty samples. We use 209 normal cases for training and the rest for testing. The Yuan Dynasty samples in the training set and test set are both randomly selected.

We adopt the gradient attention map (GRAM) [33] to extract anomalous patterns within an underlying variational graph autoencoder (VGAE) model, calculating an anomaly score for each sample. The framework of the GRAM is illustrated in Fig. 2 and Algorithm 1, consisting of two main phases: the training phase (Fig. 2a) and the testing phase (Fig. 2b). During the training phase, our approach involves unsupervised training of the underlying GNNs exclusively on the normal graph data. This training process enables the GNNs to only capture the characteristics of normal graphs, which can be interpreted by the GRAM of the entire graph representation with respect to the node feature embeddings. When the GRAM is examined during the testing phase, the GRAM of the anomalous samples will exhibit regions that are significantly different from those of the normal samples.

Algorithm 1 GRAM

Training phase:

Initialize: The parameters $\boldsymbol{\theta_0}$ of Encoder of the VGAE; the parameters $\boldsymbol{\phi_0}$ of the Decoder of the VGAE; iteration epochs $\boldsymbol{N}$.

for $\boldsymbol{i = 1, 2, \cdots, N}$ **do**

$\mathbf{Z} \leftarrow \boldsymbol{\theta_{i-1}}(\mathbf{X}, \mathbf{A})$

$\left(\widetilde{\mathbf{X}}, \widetilde{\mathbf{A}}\right) \leftarrow \boldsymbol{\phi_{i-1}}(\mathbf{Z})$

$\boldsymbol{\theta_i}, \boldsymbol{\phi_i} \leftarrow \mathbf{arg\,min}\ \boldsymbol{loss}(6)$

end for

Save the parameters $\boldsymbol{\theta_{bset}}, \boldsymbol{\phi_{best}}$ of the best model with the minimum loss.

Testing phase:

Load the parameters $\boldsymbol{\theta_{bset}}$ of the best model to Encoder of testing phase,

$\mathbf{Z} \leftarrow \boldsymbol{\theta_{best}}(\mathbf{X}, \mathbf{A})$

$\mathbf{z} = \mathbf{GlobalAddPooling}(\mathbf{Z})$

Compute the anomaly score by (11-16).

During the training phase, we utilize the VGAE model, which comprises two essential components: the encoder and the decoder. In the encoder, we first employ the GNN to extract feature representations $\mathbf{H}$ from the input graph data $\mathcal{G}$. Suppose the input graph contains N nodes with M-dimensional features for each node, its node feature matrix is denoted by $\mathbf{X} \in \mathbb{R}^{N \times M}$ and the adjacency matrix is denoted by $\mathbf{A} \in \mathbb{R}^{N \times N}$. The GNN model takes as input the node attributes $\mathbf{X}$ and the structural information $\mathbf{A}$, and generates J-dimensional output features as.

$$\mathbf{H} = \mathrm{GNN}(\mathbf{X}, \mathbf{A}), \mathbf{H} \in \mathbb{R}^{N \times J} \tag{4}$$

For the GNN model, we use a graph convolutional network (GCN) [34] with L layers, which is widely used to process graph data. For our GNN model, $\mathbf{H}^{(0)} = \mathbf{X}$ is the input feature and the output feature $\mathbf{H} = \mathbf{H}^{(L)}$. Additionally, the Gaussian Error Linear Unit (GELU) [35] is applied between the two layers of the GCN. Subsequently, two MLPs comprising two linear layers with a GELU in between are employed to generate the mean M and logarithmic standard deviation $\log\mathbf{\Sigma}$ of the I-dimensional latent variable. Then, the latent variable matrix $\mathbf{Z}$ is sampled according to.

$$\mathrm{Z} = \mathrm{M} + \mathrm{E} \odot \exp(\log \Sigma), \mathrm{Z} \in \mathbb{R}^{N \times I}, \tag{5}$$

where $\mathbf{E}$ is a white noise whose entries follow the standard normal distribution independently. Moreover, $\odot$ represents pointwise multiplication. Moving on to the decoder, it also includes two MLPs and two GNNs, which are the same as the MLPs and GNNs in the encoder, for reconstructing the node features $\mathbf{X}$ and the adjacency matrix $\mathbf{A}$, respectively, resulting in $\widetilde{\mathbf{X}}$ and $\widetilde{\mathbf{A}}$. Comparing the reconstructed $\widetilde{\mathbf{X}}$ and $\widetilde{\mathbf{A}}$ with the original inputs $\mathbf{X}$ and $\mathbf{A}$, respectively, the reconstruction error for the VGAE loss function can be derived. Specifically, the loss function for the VGAE is thus.

$$loss = \beta\|\mathbf{X} - \widetilde{\mathbf{X}}\|_{\mathrm{F}}^2 + (1-\beta)\|\mathbf{A} - \widetilde{\mathbf{A}}\|_{\mathrm{F}}^2 + \text{KL-Loss}, \tag{6}$$

where β is a hyperparameter, $\|\cdot\|_{\mathrm{F}}^2$ is the Frobenius norm, and the KL-loss is computed by.

$$\text{KL - Loss} = -\frac{1}{2N}(1_N)^{\mathrm{T}}\Big[(1_N)(1_M)^{\mathrm{T}} + 2\log\Sigma - \mathrm{M}\odot\mathrm{M} - \exp\big(2\log\Sigma\big)\Big](1_M). \tag{7}$$

Here, 1_N and 1_M represent column vectors of all ones, with dimensions N and M respectively. In the testing phase, we utilize the encoder that was trained during the training phase to obtain the latent variable matrix $\mathbf{Z}$ according to (4) and (5).

In order to get the graph level embedding, the latent vector $\mathbf{z}$ is obtained from $\mathbf{Z}$ by applying a global add pooling:

$$\mathbf{z} = \text{GlobalAddPooling}(\mathbf{Z}) = (1_N)^{\mathrm{T}}\mathbf{Z}, \mathbf{z} \in \mathbb{R}^I. \tag{8}$$

The leverages the gradients of $\mathbf{z}$ with respect to the output features $\mathbf{H}$ of the GNN model to compute the anomaly score. Specifically, we first define the gradient attention coefficients as follows:

$$\boldsymbol{\alpha}_i := \frac{1}{N}\sum_{n=1}^{N}\frac{\partial z_i}{\partial \mathbf{h}_n} \in \mathbb{R}^J, i = 1, \cdots, I, \tag{9}$$

where $z_i \in \mathbb{R}$ represents the i-th element of $\mathbf{z}$ and $\mathbf{h}_n \in \mathbb{R}^J$ represents (the transpose of) the n-th row of $\mathbf{H}$, corresponding to the n-th node. Next, we calculate the node-level anomaly scores for individual nodes as follows:

$$\mathbf{s} \equiv [s_n]_{n=1}^N := \left[\sum_{i=1}^{I}\phi\left(\boldsymbol{\alpha}_i{}^{\mathrm{T}}\mathbf{h}_n\right)\right]_{n=1}^N, \tag{10}$$

where ϕ refers to the nonlinear activation function used for producing $\mathbf{z}$. The graph-level anomaly score is then given by.

$$Score := \text{GlobalAddPooling}(\mathbf{s}) \equiv \sum_{n=1}^{N} s_n. \tag{11}$$

This anomaly score is then thresholder to determine whether to classify the graph as an anomaly, which means whether the porcelain sample was produced during the Yuan Dynasty or not.

Machine learning experimental settings

During the training phase of the VGAE, the Adam optimizer is utilized. Within the GRAM framework, essential hyperparameters are considered, including the output dimension J, which signifies the feature information of each node after GNN-based extraction, the dimension I representing the latent vector $\mathbf{z}$, the parameter β linked to the loss function (6), and the learning rate. Notably, the GNN layers are consistently configured with a consistent neuron count of J, while the MLP layers also maintain a uniform neuron count of I. Specifically, we set $J = 128$, $I = 64$, $\beta = 0.6$, and the learning rate is 0.0005.

We evaluate the GRAM against the widely used anomaly detection methods: OCSVM [15], IF [17], LOF [18], GAAN [22], OC-GNN [23], GCNAE [24], DOMINANT [25], CONAD [26], and GUIDE [27]. In relation to the baseline methods, we leverage publicly available code from [36] https://github.com/pygod-team/pygod/, while ensuring the preservation of GNN structures identical to those employed in our VGAE model. We conduct all experiments on a server powered by an Intel ® Xeon ® Gold 6226R CPU @ 2.90 GHz, complemented by NVIDIA GeForce RTX 3090 GPUs. Each experiment is executed using a singular GPU.

Results and discussion

Chemical compositions and conventional indicators

The major oxide compositions in the body, glaze, and blue area of the samples are listed in Additional file 2: Appendix S2, Additional file 3: Appendix S3, and Additional file 4: Appendix S4, respectively.

Traditionally, the Al_2O_3 and SiO_2 content of ceramic bodies are used to distinguish the origin and era [1, 13]. The samples have Al_2O_3 content ranging from 10 wt% to 30 wt%, and SiO_2 content mostly between 60 wt% and 80 wt%. The Al_2O_3 vs. SiO_2 values show a negative correlation, indicating the typical characteristics of southern Chinese porcelain with high-Si and low-Al. Previous studies found that Jingdezhen porcelain bodies with > 20 wt% Al_2O_3 in Yuan Dynasty resulted from adding kaolin into chinastone [1, 29, 30], the weathered granite outcropping in the Jingdezhen region. According to historical documentation, the ceramic body formula in Jingdezhen after the Yuan Dynasty followed the binary system of adding kaolin to chinastone [1, 2]. Therefore, the Al_2O_3 and SiO_2 compositions of the porcelain body cannot distinguish Yuan Dynasty blue and white porcelain from ancient blue and white porcelain produced in Jingdezhen (Fig. 3).

The content of alkali oxides and alkaline earth oxides is the main distinction for traditional Chinese high-temperature calcium glazes [1]. The coefficient b in the Seger formula reflects the ratio of these two groups of oxides. The form of the formula is $aR_2O{\cdot}bRO{\cdot}cR_2O_3{\cdot}dRO_2$,

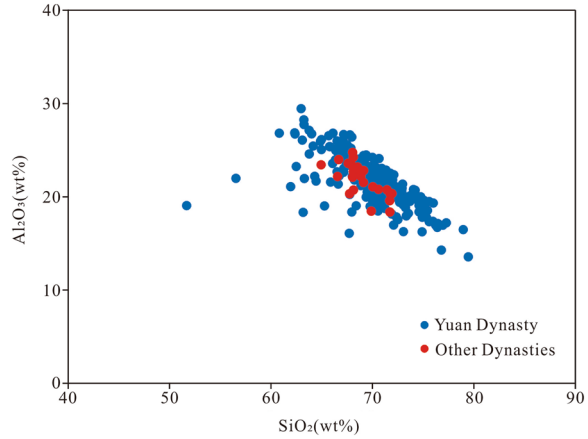

Fig. 3 Scatter diagram of SiO_2 vs. Al_2O_3 of porcelain body

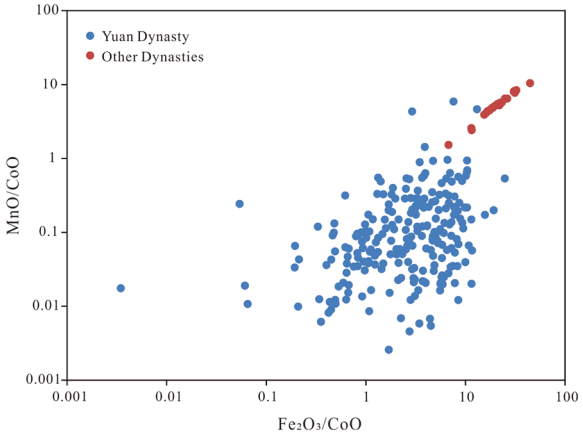

Fig. 5 Logarithmic Fe_2O_3/CoO vs. Mn/CoO plots of porcelain blue area

where R_2O and RO represent alkali oxides and alkaline earth oxides, respectively, R_2O_3 and RO_2 represent trivalent and tetravalent oxides, respectively, and the coefficients a, b, c, and d correspond to the molar quantities of each type of oxide when (R_2O+RO) equals 1.The traditional Chinese high-temperature calcium glazes can be classified into three types based on the value of coefficient b: calcium type ($b>0.75$), calcium-alkali type ($0.5<b\leq0.75$), and alkali-calcium type ($b\leq0.5$) [37]. The Yuan Dynasty samples have a wide range of coefficient b values, from alkali-calcium type to calcium type, while most of the Ming and Qing Dynasty samples are alkali-calcium type and calcium-alkali type (Fig. 4). Therefore, a low coefficient b value (<0.75) in the glaze of an ancient blue and white porcelain produced in Jingdezhen does not indicate its belonging to the Yuan Dynasty, but a high coefficient b value (>0.75) may suggest a Yuan Dynasty production time.

The values of MnO/CoO and Fe_2O_3/CoO in the blue cobalt areas can help determine their provenance by comparing them with known cobalt minerals [38–40]. Different regions have different types of raw cobalt ores. Imported cobalt ore is a mineral assemblage of Ni-Co–Cu-As-Fe formed by epithermal hydrothermal deposits [41, 42]. Domestic cobalt ores are mainly weathered and sedimentary deposits in Jiangxi, Zhejiang and Yunan provinces of China. They are small-scale deposits with heterogenites as the main Co-bearing minerals, which coexist with Fe–Mn sediments in the weathering layer [1, 43]. Therefore, the Fe–Mn-Co contents of cobalt pigments can indicate whether they are domestic or imported. The Yuan Dynasty used imported cobalt material in Jingdezhen, while the middle and late Ming and Qing Dynasties used domestic material [2, 31]. Figure 5 shows that the Yuan Dynasty samples have scattered

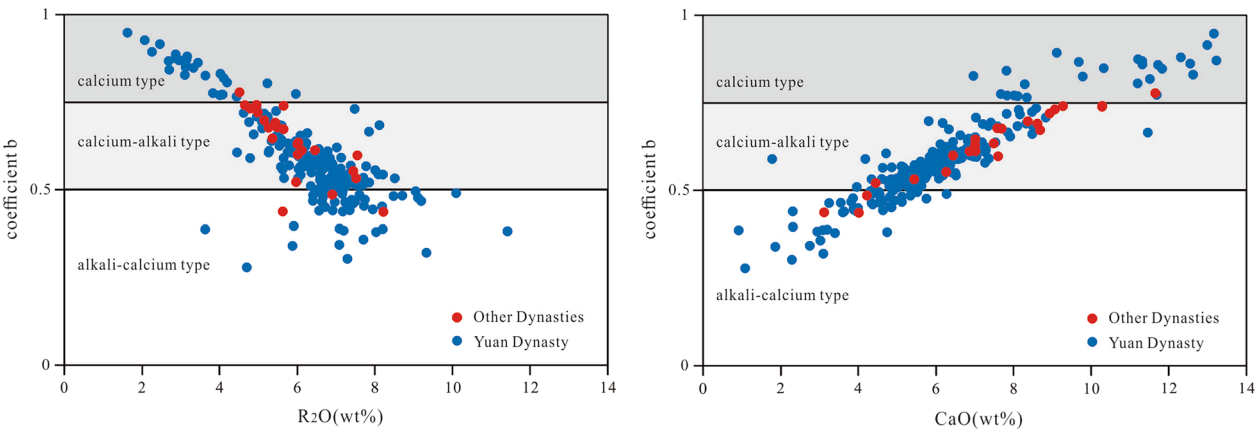

Fig. 4 Scatter diagrams of oxide vs. coefficient b of porcelain glaze. ($R_2O=Na_2O+K_2O$)

points, while the Ming and Qing Dynasty samples have a positive correlation between MnO/CoO and Fe_2O_3/CoO. This may be related to the fact that the Yuan Dynasty did not purify the cobalt material and used crushed ore directly. The imported cobalt materials used in the Yuan Dynasty were probably pre melted materials, which may have come from different regions in West Asia [42]. The MnO/CoO values of the Ming and Qing Dynasties are higher, which matches the high Mn content of domestic material. However, there is some overlap between the Yuan Dynasty and the Ming and Qing Dynasty samples, and no clear boundary can be drawn.

To summarize, the chemical compositions of the porcelain would change in different periods due to the variations in the porcelain formula and process. However, some conventional indicators based on the chemical composition cannot reliably differentiate between the blue and white porcelain of Jingdezhen in the Yuan Dynasty and the later periods.

Experimental results based on machine learning

In the testing phase, all the methods provide anomaly scores for each test sample. To assess their effectiveness, we perform a thorough evaluation of the graph-level anomaly scores using commonly used metrics such as AUC (Area under the Receiver Operating Characteristic Curve) and AP (Average Precision) scores. When determining whether a test sample is abnormal or normal, the anomaly score is compared with a threshold. This comparison enables the calculation of FPR (false positive rate: percentage of incorrectly labeled negative cases) and TPR (true positive rate: percentage of correctly labeled positive cases) for the test set. The ROC (Receiver Operating Characteristic) curve plots the FPR against the TPR from different thresholds. AUC reflects the model's ability to distinguish between positive (normal) and negative (abnormal) categories, with values closer to 1 indicating superior performance. AP, ranging from 0 to 1, averages precision across different TPRs. It measures the model's precision at various TPR levels, with higher values indicating better performance.

In order to avoid random errors, we conduct the experiments with three separate random initializations of the neural network. The ROC curves for these three experiments are shown in Fig. 6. The comprehensive results for AUC and AP scores are shown in Table 1 and Table 2, respectively, where we recall that a larger score indicates a better performance. It is worth noting that in these tables, the results for the best performing method per experiment are highlighted in bold font. In addition, we also record the mean and standard deviation (Std) of the results of the three experiments in order to compare the comprehensive performance of each method in perspective.

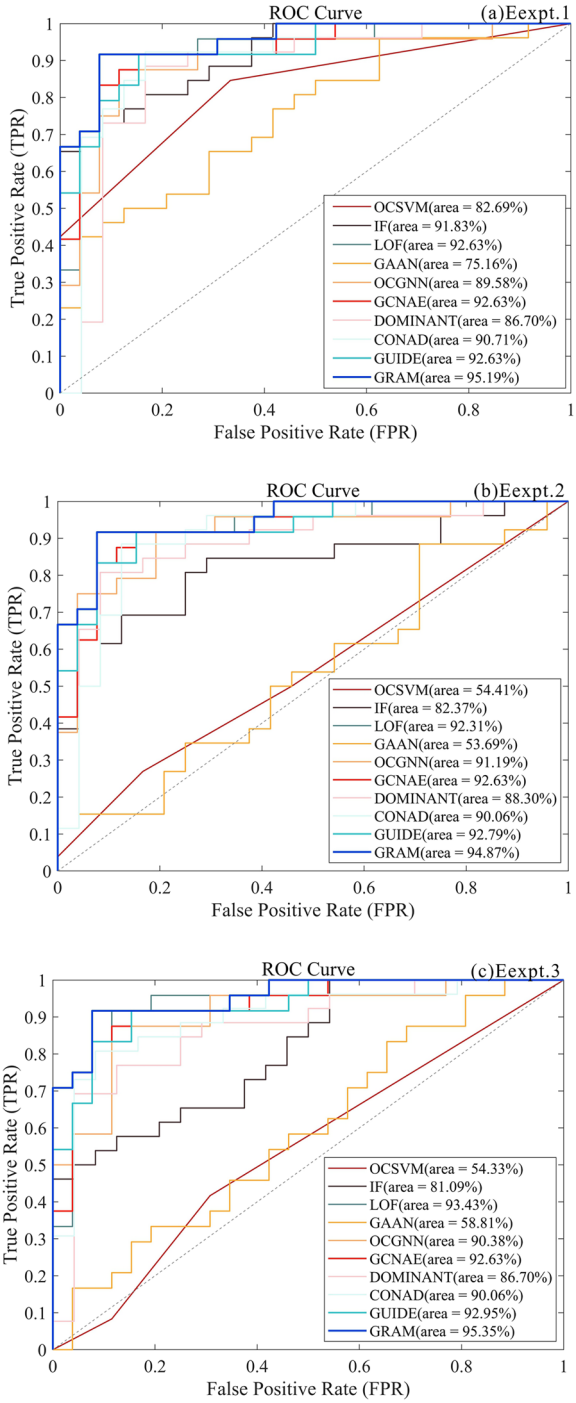

Fig. 6 The ROC curves of three experiments

Combined with Fig. 6 and Table 1, it can be observed that the GRAM performs the best on the AUC in all three experiments. In Eexpt.3, we achieved the optimal AUC with 95.35%. The average AUC of the three

Table 1 AUC results for graph-level anomaly detection

AUC	EEXPT.1	EEXPT.2	EEXPT.3	MEAN	STD
OCSVM	82.69%	54.41%	54.32%	63.81%	16.35%
IF	91.83%	82.37%	81.09%	85.10%	5.87%
LOF	92.63%	92.31%	93.43%	92.79%	0.58%
GAAN	75.16%	53.69%	58.81%	62.55%	11.21%
OCGNN	89.58%	91.19%	90.38%	90.38%	0.81%
GCNAE	92.63%	92.63%	92.63%	92.63%	0.00%
DOMINANT	86.70%	88.30%	86.70%	87.23%	0.92%
CONAD	90.71%	90.06%	90.06%	90.28%	0.38%
GUIDE	92.63%	92.79%	92.95%	92.79%	0.16%
GRAM	**95.19%**	**94.87%**	**95.35%**	**95.14%**	**0.24%**

Bold values indicate that GRAM achieves the best results compared to other methods

Table 2 AP results for graph-level anomaly detection

AUC	EEXPT.1	EEXPT.2	EEXPT.3	MEAN	STD
OCSVM	81.33%	57.03%	48.92%	62.43%	16.87%
IF	92.02%	86.66%	85.01%	88.38%	4.48%
LOF	92.81%	92.02%	92.53%	92.45%	0.40%
GAAN	79.47%	60.70%	56.86%	65.68%	12.10%
OCGNN	89.47%	91.48%	90.99%	90.65%	1.05%
GCNAE	92.58%	92.44%	92.28%	92.43%	0.15%
DOMINANT	80.44%	87.78%	85.69%	84.64%	3.78%
CONAD	85.11%	87.99%	91.29%	88.13%	3.09%
GUIDE	93.14%	93.31%	93.39%	93.28%	0.13%
GRAM	**95.48%**	**95.29%**	**95.81%**	**95.53%**	**0.26%**

Bold values indicate that GRAM achieves the best results compared to other methods

experiments also reaches 95.14%, which is the best performance among all the methods. From Table 2, we can see that the performance of the GRAM is also optimal for AP in all three experiments, and the average value of AP in the three experiments reaches 95.53%. In addition, the stability of the GRAM is also satisfactory, and the standard deviations of AUC and AP are controlled within 0.3% for the three experiments. Overall, GRAM can effectively solve this task.

Conclusion

In this study, we acquire a large dataset of chemical compositions of Yuan blue and white porcelain produced in Jingdezhen by using pXRF, and employ machine learning techniques to solve the problem of recognizing Yuan blue and white porcelain. We formulate the problem as an anomaly detection task, where we label porcelain from the Yuan Dynasty as normal samples and porcelain from other dynasties as abnormal samples. We propose an unsupervised GAD method, which is based on GNN interpretation. We train the VGAE model only on normal graphs, and then use its encoder to extract graph features and compute the anomaly scores by utilizing the GRAM of the graph representations with respect to the node feature embeddings. Finally, the GRAM achieves competitive results on the dataset compared to the baseline methods.

Our study has some limitations, as it only focuses on Yuan blue and white porcelain from Jingdezhen. We plan to extend our study to other dynasties and other ceramic producing regions.

Supplementary Information

The online version contains supplementary material available at https://doi.org/10.1186/s40494-024-01193-6.

Additional file 1: Appendix S1. Detailed descriptions of representative Yuan blue and white porcelains.

Additional file 2: Appendix S2. The chemical compositions of the body of porcelain samples.

Additional file 3: Appendix S3. The chemical compositions of the glaze of porcelain samples.

Additional file 4: Appendix S4. The chemical compositions of the blue pigment of porcelain samples.

Acknowledgements

Thanks to the Yuan Blue and White Museum of Jingdezhen Ceramic University for providing porcelain samples. We also would like to express our sincere gratitude to the Editor-in-Chief Richard Brereton and five anonymous reviewers for their valuable comments, which have greatly improved this paper.

Author contributions

JL and YY wrote the main manuscript text and prepared all figures. JL, YY, and DZ designed the experiments and performed the analysis of the data used in the manuscript. LW, QW and ZL collected samples and performed pXRF analysis. YY and DZ performed machine learning experiments. QL provided advice on the study and revised the manuscript. All authors read and approved the final manuscript.

Funding

This work was jointly funded by the National Social Science Fundation of China (No. 22&ZD245), the Science and Technology Project of Jiangxi Education Department (No. GJJ201346), the Project of Jiangxi Provincial Universities Humanities and Social Sciences Research (No. JD21083), the Jiangxi Ceramic Heritage Conservation and Imperial Kiln Research Collaborative Innovation Center Project (No. JXYY2101), and the Science and Technology Project of Jingdezhen City.

Availability of data and materials

The datasets used and analyzed during the current study are available from the corresponding author on reasonable request.

Declarations

Competing interests

The authors declare that they have no competing interest in this work.

Received: 16 November 2023 Accepted: 23 February 2024
Published online: 06 March 2024

References

1. Li JZ. History of Chinese Science and Technology: Ceramics (in Chinese). Beijing: Chinese Science Publishing; 1998. p. 364–83.
2. Ye ZM. Elements of the history of China's ceramics (in Chinese). Beijing: Light Industry Publishing House; 1989. p. 196–215.
3. Gerritsen A. The City of Blue and White: Chinese Porcelain and the Early Modern World. Cambridge: Cambridge University Press; 2020. p. 114–33.
4. Aitken MJ, Tite MS, Reid J. Thermoluminescent dating of ancient ceramics. Nature. 1964;202:1032–3.
5. Shugar AN, Mass JL. Handheld XRF for Art and Archaeology. Leuven: Leuven University Press; 2012.
6. Frahm E, Doonan RCP. The technological versus methodological revolution of portable XRF in Archaeology. J Arch Sci. 2013;40:1425–34.
7. Hunt A, Speakman RJ. Portable XRF analysis of archaeological sediments and ceramics. J Arch Sci. 2015;53:626–38.
8. Tykot RH. Using nondestructive portable X-ray fluorescence spectrometers on stone, ceramics, metals, and other materials in museums: advantages and limitations. Appl Spectrosc. 2016;70:42–56.
9. Frahm E. Ceramic studies using portable XRF: From experimental tempered ceramics to imports and imitations at Tell Mozan. Syria J Arch Sci. 2018;90:12–38.
10. LeMoine J, Halperin CT. Comparing INAA and pXRF analytical methods for ceramics: a case study with Classic Maya wares. J Arch Sci Rep. 2021;36: 102819.
11. Cui JF, Wood N, Qin DS, et al. Chemical analysis of white porcelains from the Ding Kiln site, Hebei Province. China J Arch Sci. 2012;39:818–27.
12. Mu TH, Wang F, Wang XF, et al. Research on ancient ceramic identification by artificial interlligence. Ceram Int. 2019;45:18140–6.
13. Sun HY, Liu M, Li L, et al. A new classification method of ancient Chinese ceramics based on machine learning and component analysis. Ceram Int. 2020;46:8104–10.
14. Qi Y, Qiu MZ, Jing HZ, et al. End-to-end ancient ceramic classification toolkit based on deep learning: A case study of black glazed wares of Jian kilns (Song Dynasty, Fujian province). Ceram Int. 2022;48:34516–32.
15. Scholkopf B, Williamson RC, Smola AJ, et al. Estimating the support of a high-dimensional distribution. Neural Comput. 2001;13:1443–71.
16. Erfani SM, Rajasegarar S, Karunasekera S, et al. High-dimensional and large-scale anomaly detection using a linear one-class SVM with deep learning. Pattern Recognit. 2016;58:121–34.
17. Liu FT, Ting KM, Zhou ZH. Isolation-based anomaly detection. ACM Trans Knowl Disc Data. 2012;6:1–39.
18. Breunig MM, Kriegel HP, Ng RT, et al. LOF: identifying density-based local outliers, in: Int. Conf. Manage. Data (SIGMOD). 2000;93–104.
19. Zhai S, Cheng Y, Lu W, et al. Deep structured energy based models for anomaly detection, in: 33rd Int. Conf. Mach. Learn. 2016;48;1100–1109.
20. Zong B, Song Q, Min MR, et al. Deep autoencoding gaussian mixture model for unsupervised anomaly detection, in: Int. Conf. Learn. Represent. 2018.
21. Lai CH, Zou D, Lerman G. Robust variational autoencoding with wasserstein penalty for novelty detection, in: Proc. Int. Conf. Artif. Intell. Statist. PMLR. 2023;3538–3567.
22. Chen Z, Liu B, Wang M, et al. Generative adversarial attributed network anomaly detection, in: 29th ACM Int. Conf. Inf. Knowl. Manage. 2020;1989–1992.
23. Wang X, Jin B, Du Y, et al. One-class graph neural networks for anomaly detection in attributed networks. Neural Comput Appl. 2021;33:12073–85.
24. Kipf TN, Welling M. Variational graph auto-encoders, NIPS Workshop on Bayesian Deep Learning. 2016.
25. Ding K, Li J, Bhanushali R, et al. Deep anomaly detection on attributed networks, in: SIAM Int. Conf. Data Mining. SIAM. 2019;594–602.
26. Xu Z, Huang X, Zhao Y, et al. Contrastive attributed network anomaly detection with data augmentation, in: 26th Pacific-Asia Conf. Knowledge Discovery and Data Mining (PAKDD) Springer. 2022;444–457.
27. Yuan X, Zhou N, Yu S, et al. Higher-order structure based anomaly detection on attributed networks, in: IEEE Int. Conf. Big Data (Big Data) IEEE. 2021;2691–2700.
28. Arli BD, Franci GS, Kaya S, et al. Portable X-ray fluorescence (p-XRF) uncertainty estimation for glazed ceramic analysis: Case of Iznik Tiles. Heritage. 2020;3:1302–29.
29. Wu J, Zhang ML, Hou TJ, et al. Analysis of the celadon of the Tang and the Five Dynasties unearthed from Nan Kiln and Lantian Kiln site of Jingdezhen. China Ceram Int. 2015;41:6851–7.
30. Wu J, Leung P, Li JZ, et al. EDXRF studies on blue and white Chinese Jingdezhen porcelain samples from the Yuan Ming and Qing dynasties. X Ray Spectrom. 2000;29:239–44.
31. Chen Y, Guo Y, Zhang Z. An investigation on Chinese blue and white ware and its blue pigment (in Chinese). Bull Chin Ceram Soc. 1978;6:225–41.
32. Zhang RQ, Gethin P. Provenance of the cobalt pigment used for Jingdezhen minyao blue-and-white porcelain in the early Qing dynasty. Ceram Int. 2021. https://doi.org/10.1016/j.ceramint.2021.05.303.
33. Yang Y, Wang P, He X, et al. Interpretable Graph Anomaly Detection using Gradient Attention Maps, arXiv:2311.06153. 2023.
34. Kipf TN, Welling M. Semi-supervised classification with graph convolutional networks, in: Int. Conf. Learn. Represent. 2017.
35. Hendrycks D, Gimpel K. Gaussian error linear units (GELUs), arXiv:1606.08415. 2016.
36. Liu K, Dou Y, Zhao Y, et al. BOND: Benchmarking unsupervised outlier node detection on static attributed graphs, in: 36th Int. Conf. Neural Informat. Process. Syst. 2022.
37. Luo HJ, Li JZ, Gao L. Calcium glaze division standard and its application in the study of glaze on Chinese ancient porcelain (in Chinese). Bull Chin Ceram Soc. 1995;2:50–3.
38. Xiao H, Ai Q, Cui JF. The invention of Jingdezhen porcelain's binary formula and the history of kaolin mineral exploitation (in Chinese with English abstract). Palace Museum J. 2020;5:23–33.
39. Zhu T, Ding X, Kusimba C, et al. Using laser ablation inductively coupled plasma mass spectroscopy to determine the provenance of the cobalt pigment of Qinghua porcelain from Jingdezhen in Yuan Dynasty of China. Ceram Int. 2015;41:9878–84.
40. Wen R, Pollard M. The pigments applied to Islamic Minai wares and the correlation with Chinese blue-and-white porcelain. Archaeometry. 2016;58:1–16.
41. Kuhanestani N, Mohammadi B, Alderton D. Mineralogical and geochemical studies on the Gowd-e-Morad (Ni Co, As-Cu) mineral deposit, Anarak (central Iran). Arab J Geosci. 2014;7:4779–91.
42. Colomban P, Kırmızı B, Franci GS. Cobalt and associated impurities in blue (and green) glass, glaze and enamel: Relationships between raw materials, processing, composition, phases and international trade. Minerals. 2021;11:633. https://doi.org/10.3390/min11060633.
43. Wu J, Li JZ. Multi-variate statistical analysis of the chemical compositions for bodies and glazes of Jingdezhen blue and white porcelain (in Chinese with English abstract). J Ceram. 1997;18:130–5.

Publisher's Note